JOURNAL OF MATERIALS SCIENCE 21 (1986) 4035–4042

Characterization of the interface between $(U, M)O_{2\pm x}$ and yttria–zirconia

S.P.S. BADWAL, F. T. CIACCHI
CSIRO, Division of Materials Science, Locked Bag 33, Clayton, Victoria 3168, Australia
D. K. SOOD
Microelectronics Technology Centre, Royal Melbourne Institute of Technology, Melbourne, Victoria 3000, Australia

Solid-state electrochemical cells have been prepared by co-sintering pre-reacted electrode and electrolyte materials together. The electrodes investigated were the non-stoichiometric oxides of the general formula $(U, M)O_{2\pm x}$ (M = Sc, Y) and the electrolyte used was yttria-stabilized zirconia. The specimens were characterized by X-ray diffraction, Rutherford back-scattering spectrometry, scanning electron microscopy with energy-dispersive analysis by X-rays, and optical microscopy. For M = Sc, an intermediate phase is formed at the interface and is responsible for the strong bonding of the electrode layer to the electrolyte. The thickness of the intermediate layer was about 2 to 3 μm. Considerable loss of uranium, which in some cases led to destabilization of the fluorite phase, was observed from the surface of the urania–scandia electrode layers. The intermediate phase is thought to be formed as a result of reaction between the electrolyte and volatile uranium-containing species produced by decomposition of the urania–scandia electrode material. For M = Y, no evidence for the formation of such a phase was found and the adhesion of the electrode to electrolyte was poor.

1. Introduction

The rates of redox reactions at the electrode/O^{2-} conducting solid electrolyte interface determine the ultimate performance, efficiency and speed of response of various electrochemical devices. Consequently the physical and chemical compatibility between the electrode and the electrolyte is of the utmost importance. Fully or partially stabilized zirconias are commonly used as the electrolyte material. For the electrode various metals (platinum, silver, gold, nickel, cobalt etc.) and metal oxides (e.g. $LaCoO_3$, doped In_2O_3, SnO_2, NiO etc.) have been used [1, 2]. More recently it was shown that non-stoichiometric oxides of the general formula $(U, M)O_{2\pm x}$ (M = Sc, Y, Pr, Dy) and having the fluorite structure are good electrode materials [3–5]. By incorporating these electrodes into oxygen sensors, the operating temperature of this device has been lowered to below 400° C [6]. However, adherence of the electrode films to electrolyte is extremely poor which makes their use in industrial environments unreliable. Moreover, for applications such as oxygen pumps and fuel cells, where these electrodes can be used, information on the thermal and chemical compatibility of the urania-based electrodes with the electrolyte is required. Several techniques such as sputtering, ion implantation, co-sintering and solid-state diffusion are under investigation in our laboratory for preparing compact electrode/electrolyte interfaces. In this paper interfaces prepared by one such technique, namely co-sintering electrode and electrolyte phases together, have been characterized.

2. Experimental procedures

The electrolyte used in all the preparations was a pre-reacted powder of 10 mol% Y_2O_3 + 90 mol% ZrO_2 (YSZ–10V) composition and was purchased from Viking Chemicals Ltd, DK-4591, Follenslev, Denmark. The electrode compositions investigated were $(U_{0.38}Sc_{0.62})O_{2\pm x}$ (ScU2), $(U_{0.5}Sc_{0.5})O_{2\pm x}$ (ScU1) and $(U_{0.4}Y_{0.6})O_{2\pm x}$ (YU2). These were prepared by co-precipitation of the metal hydroxides from solutions containing the respective metal salts, followed by calcination in air at 830° C (15 h) for ScU2, 1020° C (15 h) for ScU1 and 700° C (15 h) for YU2. X-ray diffraction patterns of the electrode powders after calcination showed single-phase materials with the fluorite structure.

Four sets of samples were prepared. The first set (Group A) was prepared by a co-pressing–co-sintering technique. It involved pressing the YSZ-10V powder in a 1/2 in. (12.7 mm) die at a lower pressure. The electrode powder (10, 20 or 30 mg per interface) was then spread uniformly on one or both flat faces of the loosely compacted electrolyte disc, followed by pressing at a higher pressure ($> 200\,MN\,m^{-2}$). The compacted discs were subsequently sintered in an argon atmosphere at 1300, 1350 or 1400° C. The electrode surfaces of the sintered discs showed some loss of uranium (see below). Therefore all other samples from this and other sets were embedded in freshly calcined urania–scandia or urania–yttria powder of the composition used in the respective samples and then sintered. For ScU2 electrode, specimens with all three thicknesses were prepared whereas for YU2 electrode,

0022–2461/86 $03.00 + .12

TABLE I Details of specimen preparations

Group/specimen identification	Preparation technique	Sintering temperature (° C) (± 10) (time (h))*	Electrode/electrolyte composition†
A1	Co-pressing–co-sintering	1300 (15)‡	ScU2/YSZ-10V
A2		1350 (15)†	ScU2/YSZ-10V
A3		1400 (15)‡	ScU2/YSZ-10V
A4		1400 (15)	YU2/YSZ-10V
B1	Painting co-sintering	1400 (15)	ScU2/YSZ-10V
B2		1400 (15)	ScU1/YSZ-10V
B3		1400 (15)	YU2/YSZ-10V
C1	Mixed oxide	1400 (15)	5 wt % ScU2 + 95 wt % YSZ-10V
C2		1000 (20)	50 wt % ScU2 + 50 wt % YSZ-10V
C3		1400 (15)	50 wt % ScU2 + 50 wt % YSZ-10V
C4		1400 (15)	50 wt % ScU1 + 50 wt % YSZ-10V
C5		1400 (15)	50 wt % YU2 + 50 wt % YSZ-10V
D1	Evaporation	1385 (3.5)	ScU2 on YSZ-10V
D2		1385 (5)	ScU2 on YSZ-10V
D3		1400 (15)	ScU2 on YSZ-10V
D4		1385 (15)	YU2 on YSZ-10V

*All samples except C2 sintered in an argon atmosphere.
†ScU1: $(U_{0.5}Sc_{0.5})O_{2\pm x}$, ScU2: $(U_{0.38}Sc_{0.62})O_{2\pm x}$, YU2: $(U_{0.4}Y_{0.6})O_{2\pm x}$, YSZ-10V: 10 mol % Y_2O_3 + 90 mol % ZrO_2.
‡Three thicknesses of samples prepared at these sintering temperatures.

specimens only with a thickness corresponding to 10 mg per interface were prepared.

The second set of samples (Group B) were prepared by painting a thin layer of the electrode paste in tri-ethylene glycol on pre-compacted (at a pressure of $> 200\,MN\,m^{-2}$) but unsintered discs of YSZ-10V powder. The penetration of the electrode powder into the electrolyte after painting was negligible and the electrode layer could be easily removed by gentle rubbing. The painted discs were then sintered at 1400° C in an argon atmosphere. Specimens were prepared with all three electrode compositions (Table I).

Preparation of the third set of samples (Group C) involved intimately mixing YSZ-10V and (U, M)$O_{2\pm x}$ powders in 95 : 5 or 50 : 50 weight ratio in ethanol or acetone, pressing into disc shapes followed by sintering either at 1000 or 1400° C.

The last set (Group D) of specimens were prepared by embedding the pressed but unsintered discs of YSZ-10V in freshly calcined electrode powder of either $(U_{0.38}Sc_{0.62})O_{2\pm x}$ or $(U_{0.4}Y_{0.6})O_{2\pm x}$ composition and sintering at 1400° C for different times in an argon atmosphere.

Table I gives the nomenclature, sintering temperatures and other details of specimen preparation for all groups.

The X-ray diffraction patterns of the bulk and as-prepared surfaces of various samples were recorded with a diffractometer using Cu$K\alpha$ radiation. For scanning electron and optical microscope studies of the interfaces, the samples from Groups A, B and D were cross-sectioned and polished carefully on various grades of diamond pastes. Samples (discs) from Group C were ground to a depth of several hundred micrometres and polished for examination of the phases present. X-ray mapping of the interfaces and elemental line scans across them were performed with an EDS (energy dispersive X-ray spectroscopy) attachment to the Hitachi S-450LB scanning electron microscope. Rutherford back-scattering spectrometry [7] was used to determine the depth profiles of atomic species of interest. A 2 MeV He^{2+} beam was employed at normal incidence on the target and scattering angles of 170 and 110° were used. An overall depth resolution of about 25 nm (at 170° scattering angle) was readily obtained over depths up to 1.5 μm in yttria-zirconia.

3. Results and discussion

3.1. Loss of uranium

The uncovered $(U_{0.38}Sc_{0.62})O_{2\pm x}$/YSZ-10V co-pressed–co-sintered (Table I) specimens showed the presence of a thin layer of a white powder on the electrode surface which was confirmed by X-ray diffraction to be Sc_2O_3. The amount of scandia (Sc_2O_3) increased with the sintering temperature. Apart from scandia, the only other phase detected was the urania–scandia fluorite phase. X-ray diffraction of the repeatedly ground electrode surface showed a sharp decrease in the intensities of the scandia peaks relative to the fluorite phase.

Fig. 1a shows Rutherford back-scattering (RBS) spectra of an uncovered ScU2/YSZ-10V sample before (dots) and after (solid line) sintering at 1350° C (15 h). The arrows indicate the position of surface edges for uranium and scandium. In a typical RBS spectrum [7] displaying counts against channel number, where channel number is proportional to the scattered energy, each atomic species has its own edge or surface position. The atomic species also have their own depth scales, the surface being at the highest energy and the depth increasing towards the lower energy or channel number. The depth scale is directly proportional to the energy loss after scattering and therefore to the channel number. The shaded region in Fig. 1a is a measure of the loss of uranium. This loss was maximum at the surface and increased with the sintering temperature. The thickness of the surface layer from which uranium loss occurred was estimated from RBS

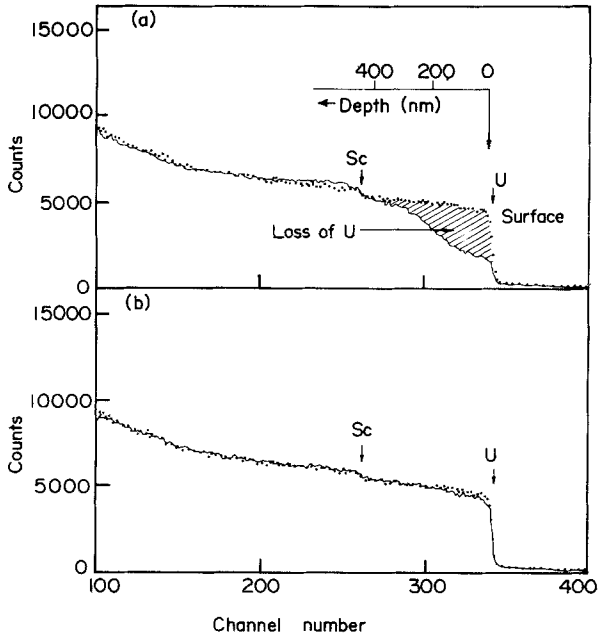

Figure 1 RBS spectra (——) of the surface of co-pressed–co-sintered discs (a) uncovered during sintering at 1350° C (15 h), (b) embedded in the electrode powder during sintering at 1400° C (15 h). The solid line in (a) and (b) is the RBS spectrum of co-pressed but unsintered disc.

spectra to be about 0.5 μm. The loss of uranium was, however, considerably reduced (Fig. 1b) when the samples were covered with ScU2 powder during sintering. For covered samples the X-ray diffractograms of the electrode surface showed only small amounts of free scandia. As a result of these observations all other samples were therefore prepared by embedding them in their respective electrode powder during sintering to avoid any uranium loss. In the case of the ScU1 electrode the loss of uranium was somewhat similar to that of ScU2 but for YU2 it was much lower than that of urania–scandia electrodes. For ScU1 no scandia and for YU2 no free yttria lines were detected in their X-ray diffractograms, although some loss of uranium was observed in all cases. The precipitation of Sc_2O_3 and the decomposition of the fluorite phase in the case of $(U_{0.38}Sc_{0.62})O_{2\pm x}$ electrode clearly occurs due to the loss of uranium and can be understood from detailed consideration of the phase diagram [8]. In the phase diagram for the urania–scandia system in air, the $(U_{0.38}Sc_{0.62})O_{2\pm x}$ composition is very close to the fluorite phase boundary limit. For higher Sc/U atom ratios the fluorite phase coexists with scandia. Thus any loss of uranium would increase the Sc/U ratio at the surface and lead to the precipitation of the scandia phase. However, for ScU1 and YU2 electrodes, the fluorite phase boundary extends to a much higher (Sc or Y)/U ratio and it is therefore highly unlikely that a small loss of uranium would lead to decomposition of the fluorite phase, as indeed was observed.

3.2. Effect of film thickness and sintering temperature

The effect of film thickness and sintering temperature was studied only for co-pressed-co-sintered specimens and for the electrode composition $(U_{0.38}Sc_{0.62})O_{2\pm x}$. The thickness of the electrode layer was estimated from scanning electron micrographs of the cross-sectioned discs. It was about 20 to 30 μm for 10 mg and 60 to 80 μm for 30 mg of the powder. These values are in agreement with those calculated based on the area, weight and density of the electrode layer. The electrode films produced by this technique are rather thick. However, with this technique it was not possible to produce much thinner films while still covering the entire electrolyte surface area uniformly at the co-pressing stage.

The thinner films prepared with 10 mg per interface electrode powder adhered firmly to the electrolyte and were free of visible surface cracks. The thicker films (20 and 30 mg per interface), although adherent to the electrolyte, developed severe surface cracks at all sintering temperatures. These electrode films along with a thin electrolyte layer adhering underneath could be easily separated from the bulk of the electrolyte disc. Scanning electron and optical examination of the cross-sectioned areas showed that even for 20 to 30 μm electrode thickness (10 mg per interface), the electrolyte had developed several cracks near the interface. The cracking of the electrolyte was much worse for thicker films and lower sintering temperatures (Fig. 2). The density of the electrolyte varied only from 92% of the theoretical for 1300° C sintering to 97% for 1400° C sintering. Most of the cracks initiated from the interface region and propagated first to a depth of 20 to 100 μm into the electrolyte and then several hundred micrometres parallel to the interface. The reasons for the cracking of the electrolyte near the interface region are not clearly obvious. During co-pressing both electrode and electrolyte phases are interlocked and macroscopic mixing of the phases can occur over several micrometres. It is quite possible

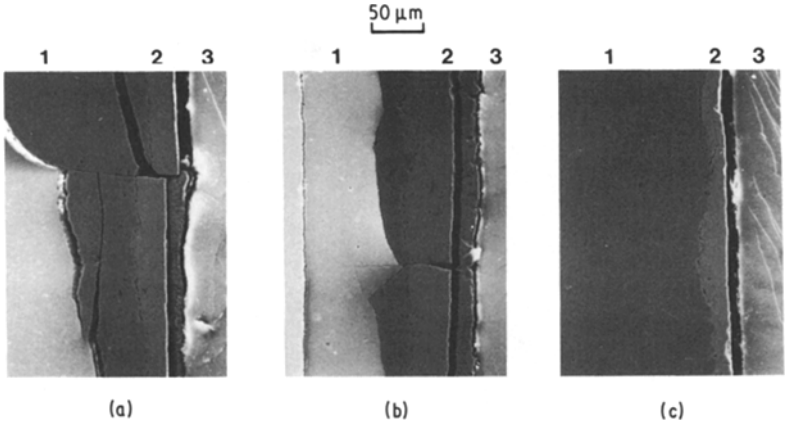

Figure 2 Scanning electron micrographs of co-pressed–co–sintered specimens (ScU2/YSZ-10V) showing cracks in the electrode and electrolyte phases after sintering at (a) 1300, (b) 1350 and (c) 1400° C for 15 h. (1) Electrolyte, (2) electrode, (3) epoxy.

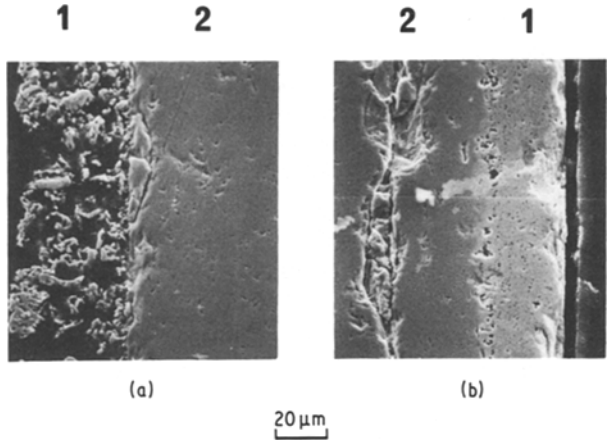

Figure 3 Scanning electron micrographs of (a) painted–co-sintered, (b) co-pressed–co-sintered ScU2/YSZ-10V interface after heat treatment of the specimens at 1400° C (15 h). (1) Electrode, (2) electrolyte.

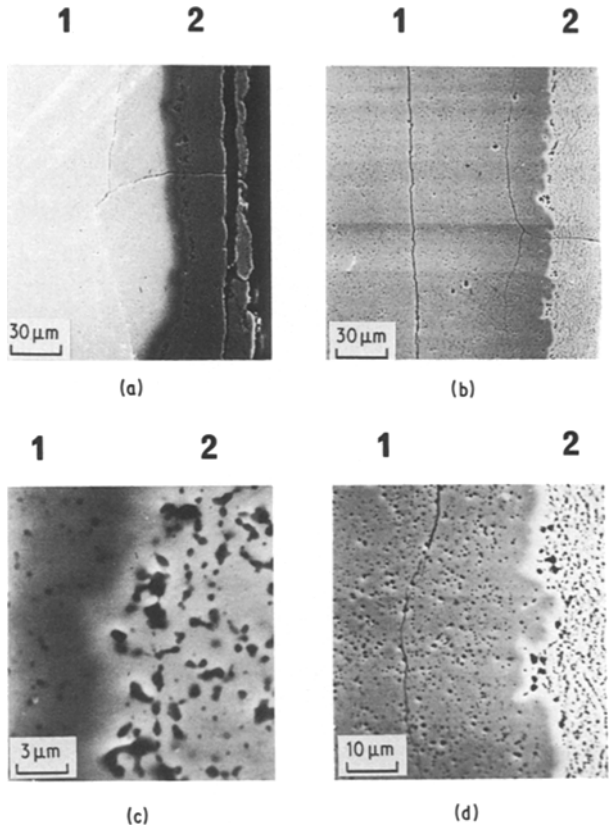

Figure 4 Scanning electron micrographs of ScU2/YSZ-10V interfaces prepared by co-pressing and co-sintering: (a) and (c) at 1350° C, (b) and (d) at 1400° C for 15 h. (1) Electrolyte, (2) electrode.

that the cracking occurs due to different sintering rates and shrinkage of both electrode and electrolyte powders, and it may not be entirely associated with the thermal expansion mismatch of the sintered phases. If the cracking had occurred during cooling due to thermal expansion mismatch of the sintered electrode and electrolyte phases alone, then similar behaviour should have been observed for all three sintering temperatures. A further evidence for this hypothesis comes from Group B samples which were prepared by painting the electrode on to unsintered discs of the electrolyte. Although these samples were sintered under identical conditions and had similar film thickness to the co-pressed-co-sintered (20 to 30 μm, the thinnest electrode layer) specimens, the cracking at the interface was far less severe (Fig. 3), as was the interlocking or mixing of phases at the interface.

3.3. Electrode/electrolyte interface

Both urania–scandia electrode compositions bonded firmly to the electrolyte irrespective of whether they were prepared by co-pressing–co-sintering or painting–co-sintering. Fig. 4 shows ScU2/YSZ-10V interfaces prepared by the co-pressing–co-sintering technique. Several observations can be made from this figure. The density of the electrode is lower than that of the electrolyte. The presence of a dense region 2 to 3 μm across (not as clear in painted samples of Group B) at the interface between yttria–zirconia and urania–scandia indicates that some reaction between the two fluorite phases has occurred. A continuous network of pores is present all along the interface between the dense region and electrode, but only in the case of co-pressed specimens. The network of pores was more conspicuous at lower sintering temperatures (Figs 2 and 4). EDS point-analysis indicates that the Sc/U ratio near the network of pores was in general higher than that in the bulk of the electrode. The dense phase region contains all the elements of the two phases, i.e. zirconium, yttrium, uranium and scandium.

The X-ray line scans for uranium, scandium and zirconium across the electrolyte/dense region/electrode are shown in Fig. 5 along with the scanning electron micrographs of the scanned area. The uranium and scandium concentration decreases very rapidly towards the electrolyte side of the dense region. The X-ray mapping of the individual zirconium and uranium elements is shown in Fig. 6. Fig. 6d was constructed as an overlap of Figs 6b and c. The overlap of the X-ray maps of uranium and zirconium clearly follows the dense region (Fig. 6a). The dense region shown above was observed in all samples prepared with both compositions of urania–scandia, irrespective of the preparation method or the sintering temperature. Thus there is sufficient evidence at this stage to suggest the existence of another phase at the interface between urania–scandia and yttria–zirconia. However, because of the limited resolution of EDS analysis, the nature and composition of this intermediate phase cannot be established.

The urania–yttria electrode, YU2, which had a composition similar to ScU2, did not adhere to the electrolyte by either co-pressing–co-sintering or painting–co-sintering techniques and there was no evidence for the formation of any intermediate phase. The electrode layer could be readily removed leaving a deep yellow coloration on the electrolyte surface. The intermediate phase therefore must be responsible for the strong adhesion of the urania–scandia electrodes to the electrolyte.

Repeated grinding and X-ray diffraction of the electrode surface for both ScUl/YSZ-10V and ScU2/YSZ-10V samples to the bare electrolyte showed only the presence of phases with the fluorite structure. In

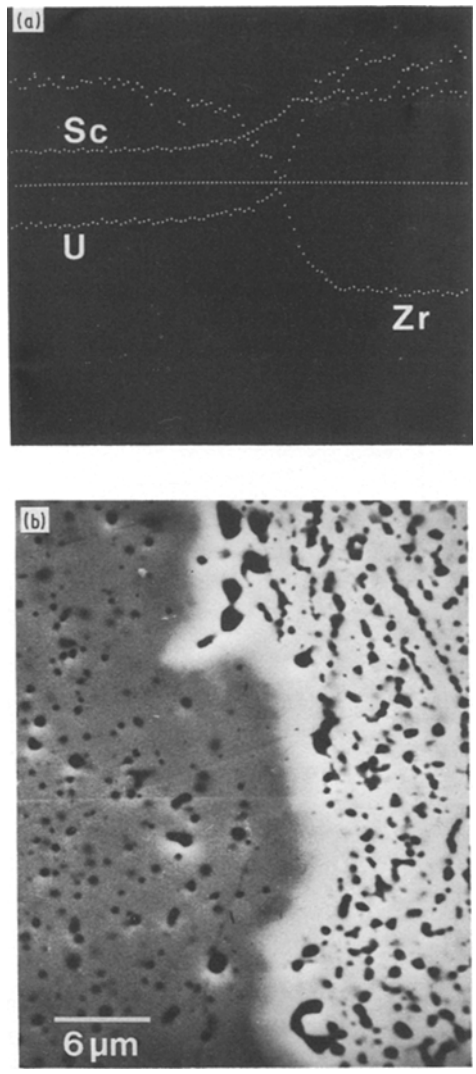

Figure 5 (a) X-ray line scans for scandium, uranium and zirconium across the ScU2/YSZ-10V interface (1400° C, 15 h), (b) scanning electron micrograph of the scanned area.

the case of ScU2 electrode a very small amount of free scandia was present throughout. Before the bare electrolyte was exposed a deep yellow coloration (compared with dark green to brownish colour of ScU1 and ScU2) on the electrolyte surface, similar to that for YU2 electrode was observed for both urania–scandia electrodes. RBS analysis of the yellow-coloured electrolyte surface from urania–scandia and urania–yttria electrodes showed only the presence of uranium, zirconium and yttrium, indicating that it is uranium which migrates into the underlying electrolyte surface.

3.4. Reaction between electrode and electrolyte phases

In order to simulate the reaction that occurs at the electrode/electrolyte interface several samples were prepared by thoroughly mixing yttria–zirconia and $(U, M)O_{2\pm x}$ powders (Group C). The 50 wt % $(U_{0.4}Y_{0.6})O_{2\pm x}$ + 50 wt % YSZ-10V (C5) disc after heat treatment at 1400° C (15 h) had a low density and very little sintering had occurred. Examination of this sample with scanning electron and optical microscopes (Figs 7a and b) showed negligible reaction between the two phases. This was further confirmed by X-ray diffraction of the disc, which showed that no shift in the fluorite peaks of either $(U_{0.4}Y_{0.6})O_{2\pm x}$ or yttria–zirconia had occurred indicating clearly that no new phase was formed. In the case of ScU1 (C4) electrode, from the X-ray diffractogram, there was clear evidence for reaction between $(U_{0.5}Sc_{0.5})O_{2\pm x}$ and yttria–zirconia. The cell parameters of $(U_{0.38}Sc_{0.62})O_{2\pm x}$ and YSZ-10V phases are too close to draw definite conclusions although some precipitation of scandia was observed. The density (% theoretical) for both urania–scandia specimens (C3 and C4) was relatively high. From scanning electron and optical microscopic examination there was little evidence of reaction at 1000° C for ScU2 (C2) (Figs 7c and d). However, after 1300° C sintering only few areas of fully unreacted yttria–zirconia were present and after the 1400° C heat treatment (C3), the reaction between the two phases seemed to be significantly advanced (Figs 7e and f).

Another experiment worth mentioning here is one performed by heating a loose mixed oxide powder of 50 wt % ScU2 + 50 wt % YSZ-10V composition at 1300° C (15 h) in an argon atmosphere. The X-ray diffractogram of the heat-treated powder showed a large precipitation of scandia compared with a pressed disc (C3) of the same composition but given a higher-temperature heat treatment. Now there was clear evidence for the formation of another fluorite phase with a cell parameter in the vicinity of 0.521 to 0.523 nm. The cell parameter for $(U_{0.38}Sc_{0.62})O_{2\pm x}$ is 0.5158 nm [9] and even lower for the yttria–zirconia phase. From the higher cell parameter of the new phase and the precipitation of scandia it appears that this phase is formed between uranium, yttrium and zirconium oxides.

The loss of uranium from the surface of uncovered co-sintered urania–scandia electrodes, the large precipitation of scandia in the case of loose mixed

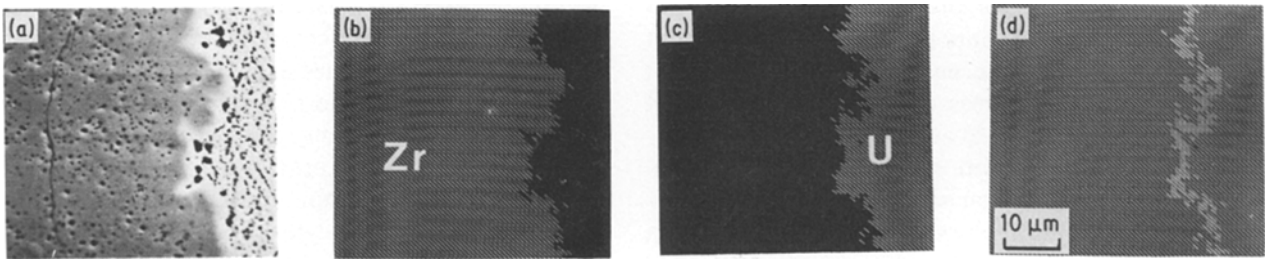

Figure 6 X-ray maps for zirconium and uranium near the ScU2/YSZ-10V interface (1400° C, 15 h) along with the mapped area.

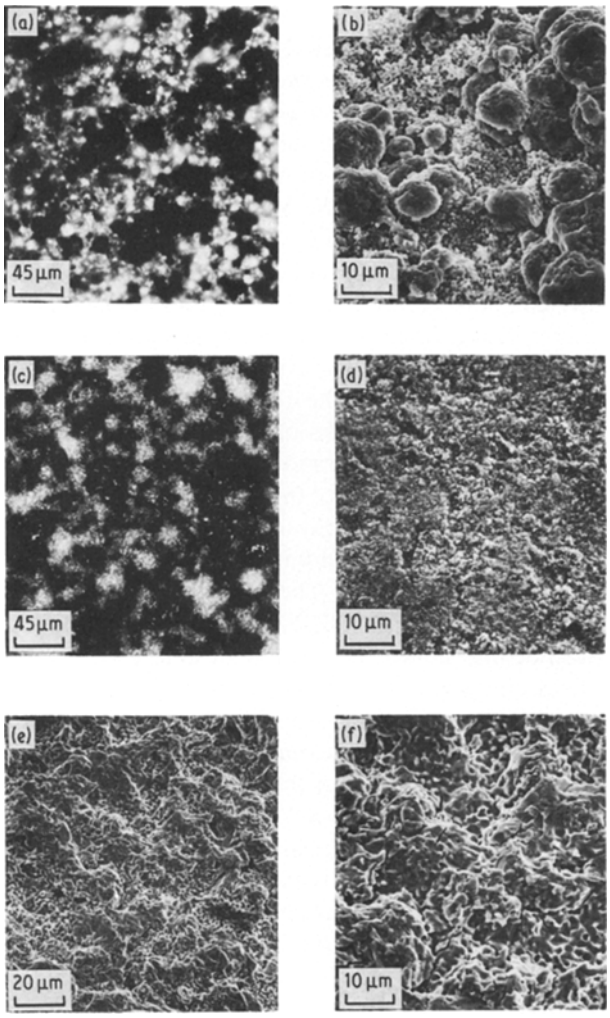

Figure 7 (b, d, e, f) Scanning electron and (a, c) optical micrographs of Group C specimens: (a, b) C5; (c, d) C2; (e, f) C3.

oxide powder (above) compared with that in the pressed discs of the same powder mix, and the yellow coloration on the electrolyte surface underneath the electrode layer, all indicate that the new phase is formed by a gas-phase reaction. The most probable mechanism for uranium loss appears to be by the following reaction:

$$UO_2 \text{ (solid solutions)} + \tfrac{1}{2}O_2(g) \rightarrow UO_3(g)$$

The $UO_3(g)$ then reacts with yttria–zirconia resulting in the formation of a new phase. In the case of pressed discs the surface area of urania–scandia exposed to ambient atmosphere for uranium loss (as $UO_3(g)$) is relatively small (in comparison with the loose powder) and is even further reduced during sintering. Therefore for pressed disc specimens (C3 and C4) the reaction cannot proceed to the degree it can in the case of loose mixed oxide powder. Point analyses of different areas of Specimens C3 and C4 indicate a complex phase assemblage with large concentration gradients and regions of compositional inhomogeneity. A similar situation but on a smaller scale would most likely exist at the urania–scandia electrode/electrolyte interface for co-pressed (Group A) and painted (Group B) co-sintered specimens.

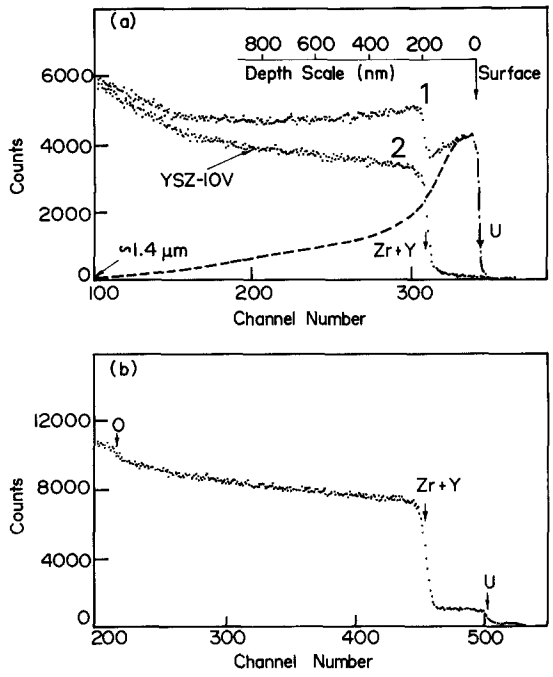

Figure 8 (a) RBS spectra of: (1) YSZ-10V disc covered with $(U_{0.38}Sc_{0.62})O_{2\pm x}$ powder during sintering at 1400° C (15 h); (2) a YSZ-10V disc sintered without any powder around it. The dashed line is an approximate depth distribution of uranium in the electrolyte. (b) RBS spectrum of YSZ-10V disc covered with $(U_{0.4}Y_{0.6})O_{2\pm x}$ powder during sintering at 1385° C (15 h).

3.5. Mechanism for the formation of the new phase

In order to gain more information regarding the mechanism, Group D samples were prepared by embedding unsintered yttria–zirconia discs in either urania–scandia or urania–yttria powders and heat-treating at 1400° C.

Fig. 8a shows the RBS spectrum (1) from a YSZ-10V disc covered with $(U_{0.38}Sc_{0.62})O_{2\pm x}$ powder during sintering at 1400° C (15 h) in an argon atmosphere. A spectrum from a YSZ-10V disc sintered at 1400° C but without any powder around it is also shown (2) for comparison. The arrows indicate the position of surface edges for uranium, zirconium and yttrium. The depth scale for uranium in zirconia shown in Fig. 8a was calculated from standard RBS analysis [7]. It is clear from Fig. 8a that a considerable amount of uranium is taken up by the yttria–zirconia disc from the powder during heat treatment at 1400° C. However no observable amount of scandium is transferred. The dashed line is an approximate depth distribution of uranium in YSZ-10V. Such a depth profile could arise from either solid-phase diffusion of uranium from the powder into YSZ or from a progressive growth of a second phase by gas-phase transfer of uranium. RBS results from samples (covered with ScU2 powder) sintered for different times show that uranium take-up is not due to simple solid-phase diffusion of uranium, since no unique diffusion coefficients can be derived from measured depth profiles of uranium. In fact RBS data indicated a non-uniform concentration of uranium on the electrolyte surface depending upon whether the electrolyte surface was covered properly with the ScU2 powder or not. This is shown in Fig. 9

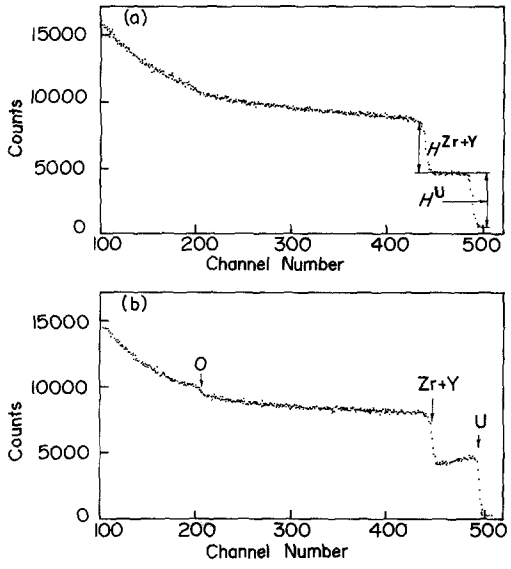

Figure 9 RBS spectra of (a) upper and (b) lower sides of a YSZ-10V disc covered with $(U_{0.38}Sc_{0.62})O_{2\pm x}$ powder (Specimen D1) during sintering at 1385° C (3.5 h).

for Sample D1 (3.5 h heat treatment at 1385° C). One side of the YSZ-10V disc had a uniform concentration of uranium at all depths down to 200 nm (Fig. 9a) whereas for the second side the uranium concentration tapered off from the surface (Fig. 9b). These results clearly show that the uranium migration results in a progressive growth of a second phase rich in uranium.

The relative amount of uranium take-up by yttria–zirconia substrate can be obtained from RBS spectra as the ratio of spectrum heights, H^{U}/H^{Zr+Y}, at the same depth, as shown in Fig. 9. The relative amounts of uranium take-up are shown in Table II for various times. Included in this table are also the data from a YSZ-10V disc covered with $(U_{0.4}Y_{0.6})O_{2\pm x}$ powder and heated at 1385° C (15 h). The relative uranium take-up increases corresponding to an increase in the volume fraction of the uranium-rich second phase (or an increase in the uranium concentration in the second phase, or both). On the other hand, uranium take-up from urania–yttria powder is much smaller (about one twentieth) for similar sintering conditions (see also RBS spectra, Fig. 8b).

The X-ray diffractograms of the surfaces of Specimens D1 to D3 also support the conclusions drawn from the RBS data, and clearly show the formation of another fluorite phase with cell parameters larger than that of either urania–scandia or zirconia–yttria. The cell parameter for the new phase increased with sintering time, consistent with increased solution of uranium in yttria–zirconia.

TABLE II Relative amount of uranium take-up by YSZ-10V for different heat-treatment conditions

Composition of the powder covering YSZ-10V	T (° C)	Time (h)	H^{U}/H^{Zr+Y} (± 0.03)*
$(U_{0.38}Sc_{0.62})O_{2\pm x}$ (D1)	1385	3.5	1.03[a], 1.06[b]
$(U_{0.38}Sc_{0.62})O_{2\pm x}$ (D2)	1385	5	1.02[a], 0.95[b]
$(U_{0.38}Sc_{0.62})O_{2\pm x}$ (D3)	1400	15	2.60
$(U_{0.4}Y_{0.6})O_{2\pm x}$ (D4)	1385	15	0.12

*(a) denotes upper face and (b) lower face of same sample.

Both RBS and X-ray diffraction results supplement earlier observations that the urania–scandia fluorite solid solutions are relatively unstable at high temperatures (> 1200° C). In the presence of oxygen considerable loss of uranium, most likely in the form of UO_3(g), occurs. The uranium species in the vapour phase then react preferentially with adjacent grains of yttria–zirconia resulting in the formation of fluorite solid solutions. It should be mentioned here that during these experiments the deposition of uranium on the walls of the alumina boat, in which the specimens were heated, was negligible. The existence of a wide range of fluorite solid solutions in the U–Zr–O, U–Zr–Y–O and related systems is well known [10, 11] and it is not surprising that such solid solutions formed in the present study. What is more intriguing is the fact that they form only when urania–scandia and yttria–zirconia phases are brought together and not in the case of urania–yttria and yttria–zirconia.

Aitken and Joseph [12] in their thermodynamic study of the solid solutions between uranium oxide and yttrium oxide concluded that there was a large negative departure from Raoult's law for the UO_2 activity in the solid solution. These deviations were much larger than those observed with UO_2–ThO_2–O_2 solid solutions. Wilson *et al.* [13] in an earlier study on the stabilization of UO_2 showed that the loss of uranium was considerably lower from solid solutions containing a trivalent additive (such as Y_2O_3, La_2O_3) in comparison with those containing a tetravalent additive (e.g. ThO_2). On the basis of this discussion one would expect less loss of uranium from both urania–scandia and urania–yttria solid solutions compared with U_3O_8 or urania–thoria although no direct thermodynamic data are available for urania–scandia fluorite solid solutions. The large volatility of uranium from urania–scandia solid solutions may be associated with the small radius of Sc^{3+}. The difference in the size of uranium and scandium cations may lead to high strain energy and low interaction energy between molecular units involving the two cations.

Preliminary investigations of the electrode/electrolyte interface indicate that the presence of an intermediate phase in the case of urania–scandia electrodes has a detrimental influence on the electrochemical behaviour [14].

4. Conclusions

The urania–scandia fluorite solid solutions show very high volatility for uranium. The loss of uranium can lead to precipitation of scandia and decomposition of the fluorite phase. The high volatility of uranium from these solid solutions is also the cause for the formation of another phase between the electrolyte and uranium. The composition of the intermediate layer formed at the interface between these materials and yttria–zirconia electrolyte is complex. The adherence of the electrode to electrolyte is improved by the formation of this new phase which leads to poor electrochemical behaviour. The urania–scandia electrodes are therefore unsuitable for applications which require the electrode/electrolyte interface to be heated above 1100 to 1200° C either during fabrication or subsequent

operation. The urania–yttria composition showed very little loss of uranium and no new phases were formed. The co-sintering technique was essentially ineffective in solving the electrode/electrolyte adherence problem.

Acknowledgements

The authors are thankful to Dr J. Drennan for helpful discussions.

References

1. H. OBAYASHI and T. KUDO, "Solid State Chemistry of Energy Conversion and Storage", edited by J. B. Goodenough and M. S. Whittingham (American Chemical Society, Washington, DC, 1977) p. 316.
2. Proceedings of Workshop on High Temperature Solid Oxide Fuel Cells, edited by H. S. Isaacs, S. Srinivasan and I. L. Harry (US Department of Energy, BNL 50756/TID-4500, 1977).
3. S. P. S. BADWAL, *J. Electroanal. Chem.* **146** (1983) 425.
4. *Idem, ibid.* **161** (1984) 75.
5. S. P. S. BADWAL, M. J. BANNISTER and M. J. MURRAY, *ibid.* **168** (1984) 363.
6. S. P. S. BADWAL and F. T. CIACCHI, *J. Appl. Electrochem.* **16** (1986) 28.
7. W. K. CHU, J. W. MAYER and M.-A. NICOLET, "Backscattering Spectrometry" (Academic Press, New York, 1978).
8. C. KELLER, U. BERNDT, M. DEBBABI and H. ENGERER, *J. Nucl. Mater.* **42** (1972) 23.
9. S. P. S. BADWAL, PhD thesis, Flinders University of South Australia (1977).
10. J. H. HANDWORK, G. D. WHITE and D. C. HILL, *J. Amer. Ceram. Soc.* **46** (1963) 29.
11. A. N. BELOV, S. I. LOPATIN, G. A. SEMENOV and I. V. VINOKUROV, *Russ. J. Inorg. Chem.* **20** (1984) 384.
12. E. A. AITKEN and R. A. JOSEPH, *J. Phys. Chem.* **70** (1966) 1090.
13. W. B. WILSON, C. A. ALEXANDER and A. F. GERDS, *J. Inorg. Nucl. Chem.* **20** (1961) 242.
14. S. P. S. BADWAL, F. T. CIACCHI and D. K. SOOD, *Solid State Ionics* **18/19** (1986) 1033.

Received 16 December 1985
and accepted 11 February 1986